A&A 623, A120 (2019)
https://doi.org/10.1051/0004-6361/201833959

Astronomy & Astrophysics

Interpretation of heliocentric water production rates of comets

D. Marshall[1,2], L. Rezac[1], P. Hartogh[1], Y. Zhao[3], and N. Attree[4]

[1] Max-Planck-Institut für Sonnensystemforschung, Justus-von-Liebig-Weg 3, 37077 Göttingen, Germany
e-mail: marshall@mps.mpg.de
[2] Universität Göttingen, Friedrich-Hund-Platz 1, 37077 Göttingen, Germany
[3] Key Laboratory of Planetary Sciences, Purple Mountain Observatory, Chinese Academy of Sciences, Nanjing, PR China
[4] Earth and Planetary Observation Centre, Department of Biological and Environmental Sciences, University of Stirling, UK

Received 26 July 2018 / Accepted 30 January 2019

ABSTRACT

Aims. We investigate the influence of three basic factors on water production rate as a function of heliocentric distance: nucleus shape, the spin axis orientation, and the distribution of activity on a comet's surface.
Methods. We used a basic water sublimation model driven by solar insolation to derive total production rates for different nuclei shapes and spin axis orientations using the orbital parameters of 67P/Churyumov-Gerasimenko. We used known shape models derived from prior missions to the Jupiter Family and short period comets. The slopes of production rates versus heliocentric distance were calculated for the different model setups.
Results. The standard (homogeneous) outgassing model confirms the well-known result regarding the heliocentric dependence of water production rate that remains invariant for different nuclei shapes as long as the rotation axis is perpendicular to the orbital plane. When the rotation axis is not perpendicular, the nucleus shape becomes a critically important factor in determining the water production curves as the illuminated cross section of the nucleus changes with heliocentric distance. Shape and obliquity can produce changes in the illuminated cross section of up to 50% over an orbit. In addition, different spin axis orientations for a given shape can dramatically alter the pre- and post-perihelion production curves, as do assumptions about the activity distribution on the surface. If, however, the illuminated cross section of the nucleus is invariant, then the dependence on the above parameters is weak, as demonstrated here with the 67P/Churyumov-Gerasimenko shape. The comets Hartley 2 and Wild 2 are shown to yield significantly different production curve shapes for the same orbit and orientation as 67P/CG, varying by as much as a factor of three as a result of only changing the nucleus shape. Finally, we show that varying just three basic parameters, shape, spin axis orientation, and active spots distribution on the surface can lead to arbitrary deviations from the expected inverse square law dependence of water production rates near 1 au.
Conclusions. With the results obtained, we cannot avoid the conclusion that, without prior knowledge of basic parameters (shape, spin axis orientation, activity locations), it is difficult to reveal the nature of cometary outgassing from the heliocentric water production rates. Similarly, the inter-comparison of water production curves of two such comets may not be meaningful.

Key words. comets: general

1. Introduction

Comets are icy bodies that heat up as they approach the Sun and sublimate volatile material from their nuclei to create a surrounding tenuous gas coma. Water vapour is generally the dominant component of the coma, especially close to the Sun (within 2 au) (Bockelée-Morvan et al. 2002; Hässig et al. 2015), however, at larger heliocentric distances where it is colder and the water ice is more stable, more volatile species such as CO can dominate the coma, as is the case for 29P/Schwassman-Wachmann (Bockelée-Morvan et al. 2010). Biver et al. (1997) show that for comet Hale-Bopp, the outgassing transitions from CO to OH dominated at approximately 3.5 au and Laeuter et al. (2019) show that the water production rate can be lower than the production rates for CO and CO_2 from 67P/Churyumov-Gerasimenko beyond 3.5 au post-perihelion. The water production rate, Q (molec. s^{-1}), increases as the distance between the nucleus and the Sun decreases due to increasing solar flux, nearly with an inverse square law dependence, but this is heliocentric-distance dependent: for volatile ices such as CO and CO_2, the production rates can be theoretically approximated by an inverse square law (r_h^{-2}) at distances less than ~4 au; for water, which has a higher sublimation temperature, the slope is usually much steeper between 1 and 4 au, and only approaches r_h^{-2} within 1 au of the Sun (Cowan & A'Hearn 1979). As noted in Steckloff et al. (2015) and Steckloff & Jacobson (2016), their model's production rate curve approaches r_h^{-2} within 2 au, but after fully considering the temperature dependence of the sublimation coefficient (Gundlach et al. 2011), the curve approaches an inverse square law within 1 au. A detailed analysis of impacts on outgassing flux due to temperature-dependent coefficients of sublimation and condensation in terms of stationary two-layer thermophysical models is also presented in Kossacki et al. (1999).

Cometary water production rate curves are unique for each object and show few common features. Some comets exhibit reasonably symmetric water production rates around perihelion (Hale-Bopp; Kührt 1999), while others show asymmetric behaviour (67P/Churyumov-Gerasimenko; Hansen et al. 2016). In addition, the peak production does not necessarily occur at perihelion as it approximately does for 2P/Encke and 46P/Wirtanen, but it can be offset to appear post-perihelion (as for 6P/d'Arrest and 30P/Reinmuth 1) or even pre-perihelion (as for 22P/Kopff and 81P/Wild 2; Bondarenko & Medvedev 2011).

The observed slopes for the water production rate also vary between comets. From the Rosetta mission, several attempts have been made to estimate the slopes for the change in the water production rate with heliocentric distance ($Q \sim r^N$) for 67P/CG (Hansen et al. 2016; Wedlund et al. 2016; Marshall et al. 2017), giving values of $N = -5.3, -3.8$, and -7.1 pre-perihelion, and $N = -7.1$ and -4.3 post-perihelion. Values for N have also been obtained for other comets, including Hale-Bopp ($N = -1.88$, Russo et al. 2000) and 153P/Ikeya-Zhang ($N = -3.21$, Russo et al. 2004). It is worth pointing out that all of these values have been obtained over different ranges of heliocentric distance.

Although suitable from an observational point of view, we raise a question: what is the exact physical relevance of these slopes to the activity and given nucleus? And how can slopes for different comets be compared?

In particular, we explore how the three basic factors – nucleus shape, obliquity of the rotation axis, and activity distribution – affect the water production rate of comets and their respective slopes[1]. It has been known for a long time (Sekanina 1981) that the orientation of the spin axis is very important for the light curves (brightness) of comets, with highly oblique objects like 6P/d'Arrest being able to sustain their brightness weeks after perihelion. We also discuss how our simplified model can be improved to add further realism. However, with more free parameters added to the problem it is unlikely that we can break the demonstrated degeneracy, if at least the basic nucleus shape, spin axis orientation, and the active spot distributions are unknown.

2. Sublimation model

Following works such as Watson et al. (1962), Cowan & A'Hearn (1979), Weissman & Kieffer (1981), and Steckloff et al. (2015), the sublimation of water per unit area from an icy body can be written as

$$\frac{S_o(1-A_v)}{r_h^2} = \epsilon\sigma T^4 + Z(T)L_{\rm ice}, \tag{1}$$

where S_o is the solar flux with a value of 1367 $\mathrm{Wm^{-2}}$ at 1 au, A_v is the bolometric Bond albedo with a value of 0.01 (Lamy et al. 2007), r_h is the heliocentric distance (dimensionless), ϵ is the emissivity with a value of 0.9, σ is the Stefan-Boltzmann constant, T is the surface ice temperature, $Z(T)$ is the sublimation rate (kg $\mathrm{s^{-1}}$ $\mathrm{m^{-2}}$), and $L_{\rm ice}$ is the latent heat of water ice with a value of 2.6×10^6 $\mathrm{J\,kg^{-1}}$, taken to be a constant. This is similar to the form given in Keller et al. (2015). The rate of sublimation can be calculated from the equations (Fanale & Salvail 1984; Langmuir 1913)

$$Z(T) = 2P(T)/(\pi v_{\rm th}(T)), \tag{2}$$

$$P(T) = 3.56 \times 10^{12} \exp(-6141.667/T)\ (\mathrm{kg\,m^{-1}\,s^{-2}}), \tag{3}$$

$$v_{\rm th}(T) = \sqrt{8RT/\pi\mu}. \tag{4}$$

The constants in Eq. (3) are from solving the Clausius-Clapeyron equations. The thermal velocity (the mean of the magnitude of the molecular velocities) is represented by $v_{\rm th}$, R is the gas constant, and μ is the molar mass of water.

The water production rate is simply the product of the sublimation rate of a region, $Z_{\rm region}(r_h)$, and the sublimating area of the region, $A_{\rm region}$. As we only use digital shape models in this work, the regions we describe are the triangular facets of a shape model. Summing over all facets, where N is the number of facets and i is the ith facet, gives the total water production rate of

$$Q(r_h) = \Sigma_i^N Z_i(r_h) A_i. \tag{5}$$

For the sake of simplicity and to isolate the effects of spin axis orientation, shape, and the distribution of activity on the surface, Eq. (1) is presented only for highly idealised conditions of pure surface ice with zero thermal inertia. For the same reason we also neglect the temperature dependence of the sublimation coefficient (Gundlach et al. 2011), which may lead to overestimating the water production rate within ~1 au by a factor of five (Steckloff et al. 2015). We assume that the cometary objects in this work are only made of water ice. These idealistic simplifications limit the validity of our model to heliocentric distances up to ~3–4 au (Meech et al. 2004). At larger distances, the heat conductivity term becomes significant and is dominated by the radiative part (Skorov et al. 2017). However, for detailed modelling, the composition, structure, and microphysical properties of the near surface layer must be known. We acknowledge that cometary activity is more complex than assumed here (the so-called Whipple model; Whipple 1950), and additional process such as ice phase changes near the sub-surface, extended sources (such as inferred for 103P/Hartley2), and super-volatile releases have an impact on water production rates, as does their surface distribution. Nevertheless, all of these remain poorly constrained apart from a few comets visited by spacecrafts (usually over a limited r_h range) and would only add unnecessary complexity and additional unconstrained parameters.

With the stated assumptions, when the total flux term (the left side of Eq. (1)) is low, most of the energy goes into the thermal re-radiation term, and the sublimation term is negligible. As the total flux increases, more energy goes into sublimation and from approximately 50–1000 $\mathrm{Wm^{-2}}$ (or 160–200 K surface temperature) the sublimation and thermal re-radiation terms on the right side are both similar in magnitude. At heliocentric distances less than 1.2 au, the flux can be greater than 1000 $\mathrm{Wm^{-2}}$ (or 200 K surface temperature), and then the sublimation flux accounts for more than 90% of the total flux and dominates over the thermal re-radiation term. When the flux is large (>1000 $\mathrm{Wm^{-2}}$), the thermal term does not contribute much, and Eq. (1) reduces to

$$\frac{S_o(1-A)}{r^2} \approx \frac{Q}{A} L_{\rm ice}, \tag{6}$$

replacing Z with Eq. (5). It can be seen that for large fluxes, for instance when a comet is close to the Sun, the water production rate follows an inverse square law for the heliocentric distance.

For the numerical modelling described in this work, we used the sublimation model in Eq. (1) to calculate the received flux and hence water production rate for a comet on an orbit around the Sun. We used a 67P-like orbit (eccentricity = 0.64, semimajor axis = 3.46) and changed the shape of the object on the orbit. For every facet of an object, the received flux can simply be calculated from the heliocentric distance and the orientation of the facet normal vector and the Sun vector. Although important for very precise modelling of activity, shadowing and self-heating are not included in our considerations of real-shape illumination conditions. The inclusion of self illumination only makes small changes to the water production rate of 67P inside ~3 au (Keller et al. 2015). The received flux then corresponds to a temperature and sublimation rate given in a pre-calculated lookup table. The production rate for each facet is found by multiplying the facet sublimation rate by the facet area. The orbit is divided into

[1] The Python code used in this paper is available to download from https://gitlab.com/david_marshall_mps/comet-outgassing-QvRh

fifty intervals and at each interval the temperature, sublimation rate, and production rate are determined for every facet over a single comet rotation. The average sublimation and production rates are then calculated for each heliocentric distance by averaging over all facets over one rotation. For simplicity we neglected the effects of self-heating for irregular shapes, which does not invalidate the main points of this work as demonstrated in Keller et al. (2015).

The model does not need to account for a rotation rate. At each heliocentric distance interval, the comet is simply rotated and the water production is calculated for each interval during a comet day. We assumed a fast rotator such that the rotation period is short and during one rotation, the heliocentric distance does not change significantly.

This enables us to probe the effects of different shapes on the change in production rate with heliocentric distance. We also investigated the effect of the obliquity angle, defined as the angle between the rotation axis and the normal to the orbital plane, with the rotation axis in the same direction as the semi-major axis. In addition, we consider Φ, the argument of the subsolar meridian at perihelion (hereafter, called argument Φ) defined as the angle swept out by the rotation axis from the semi-major axis (Sekanina 1981). Obliquity and argument Φ are rotations of the spin axis in two different perpendicular planes. We chose this method to demonstrate the effects of these two angles of axis orientation separately. Finally we studied the effect of random and non-random distributions of activity on the surface.

3. Results

3.1. Effect of comet shape and obliquity

We used five known comet shapes (67P – Preusker et al. 2015, 81P/Wild2 – Farnham et al. 2005, 103P/Hartley 2 – Farnham & Thomas 2013a, 1P/Halley – Stooke 2002, and 9P/Tempel 1 – Farnham & Thomas 2013b) as well as a sphere model and solved Eq. (1) for each elementary facet of each comet around a 67P-like orbit. This was done for obliquity values of 0°, 30°, 45°, 60°, and 90°, keeping Φ constant (equal to 0). These obliquity values do not match the true rotation axis orientations of these comets, our motivation is only to scan this parameter range to isolate its effects as a function of nucleus shape.

We note that these shape models come from a variety of space mission flybys, which do not have full coverage and provide at best only tens of metre resolution (except for the 67P shape model). However, we are only interested in how the overall shape (illuminated cross-section) affects the production rate curve. Therefore, we consider the detailed morphological inaccuracy and limited resolution of the shape models to not be significant for the conclusions derived in this work.

The change in the normalised cross section of the illuminated active area for each comet at each obliquity is shown in Fig. 1. Each curve is normalised to its maximum value. We define the cross section of the active illuminated area, A, as a summation over all facets:

$$A = \Sigma\, A_{\rm f} \cos(\theta_{\rm f}), \tag{7}$$

where $A_{\rm f}$ is the area of a single facet and $\theta_{\rm f}$ is the angle between the facet normal vector and the Sun-facet vector. If the angle is greater than 90°, it is set to 90° so that the flux is zero for non-illuminated facets.

For the spherical comet, the illuminated area does not change with heliocentric distance for any obliquity. In fact, regardless of shape, at 0° obliquity the cross section of the active illuminated area is constant for any object with heliocentric distance. Despite 67P's irregular shape, its illuminated area does not change much, dropping by only 5% for an obliquity of 90°.

When the rotation axis has a large obliquity angle, the nucleus shapes of 81P/Wild 2 and 9P/Tempel 1 cause significant changes in the illuminated area during an orbit. Additionally, the larger the obliquity angle of the rotation axis is, the larger the change in area. For both comets, the illuminated area decreases on approach to the Sun before suddenly increasing again within 1 au from perihelion.

Similarly, for 103P/Hartley 2 and 1P/Halley, the elongated shapes of the nucleus result in changes in the illuminated area, this time increasing on perihelion approach and then rapidly decreasing before closest approach. For these two comets, the (illuminated) area changes by more than 50% from maximum to minimum.

The change in the illuminated area with heliocentric distance has a profound effect on the production rate curves, as seen in Fig. 2. Distance from perihelion is the difference between the comet heliocentric distance and the perihelion distance (1.24 au for 67P). The production rate for a sphere at 0° obliquity is shown in dark blue, and the gradient of the production rate curve is shown in the bottom panels. A comet of any shape at 0° obliquity exhibits a very similar normalised production rate and slope, and a sphere at any obliquity also gives the same normalised result. There are slight fluctuations in the change in illuminated area. This is because the sphere has been decomposed into facets and due to the low resolution sphere used here, there are negligible changes in the illuminated area.

The results for 67P at a rotation axis angle of 60° are in light blue. Even though we consider a large obliquity angle, the production rate curve and the corresponding slopes do not change much in comparison to the spherical case with no axial tilt. Despite the shape and obliquity of 67P, it exhibits similar behaviour to a sphere, as a result of its coincidental invariance of illuminated cross section with inclination.

The dark and light orange lines in Fig. 2 represent the production rate and slopes for 81P/Wild 2 and 103P/Hartley 2, respectively, at 60° obliquity. In contrast to 67P, these comets yield notable changes in production rates and gradients when obliquity changes, which is due to their shapes that do result in changes of total illuminated area.

In the example for 103P/Hartley 2, the area starts to increase from large heliocentric distances until it reaches a maximum and then decreases in the final approach to perihelion. As a result, the production rate curve is steeper than the other cases far from the Sun but less steep close to the Sun, and the slope even becomes positive at perihelion. The increasing flux as the comet approaches the Sun should increase the production rate but the decreasing illuminated area means that there is less flux available for sublimation.

For Wild 2, the opposite behaviour occurs. The illuminated area starts to decrease from large heliocentric distances until it reaches a minimum and suddenly increases as it approaches perihelion. The sudden increases in area result in steeper production rate slopes around perihelion than for any of the tested objects and obliquity setup. In this case, not only does the flux increase for the comet, but also the area, so the increase in water production is enhanced and the slope is steeper.

It is therefore evident that, before even considering any properties of the comet nucleus, the water production rates and their corresponding slopes are heavily dependent upon the obliquity of the rotation axis and shape.

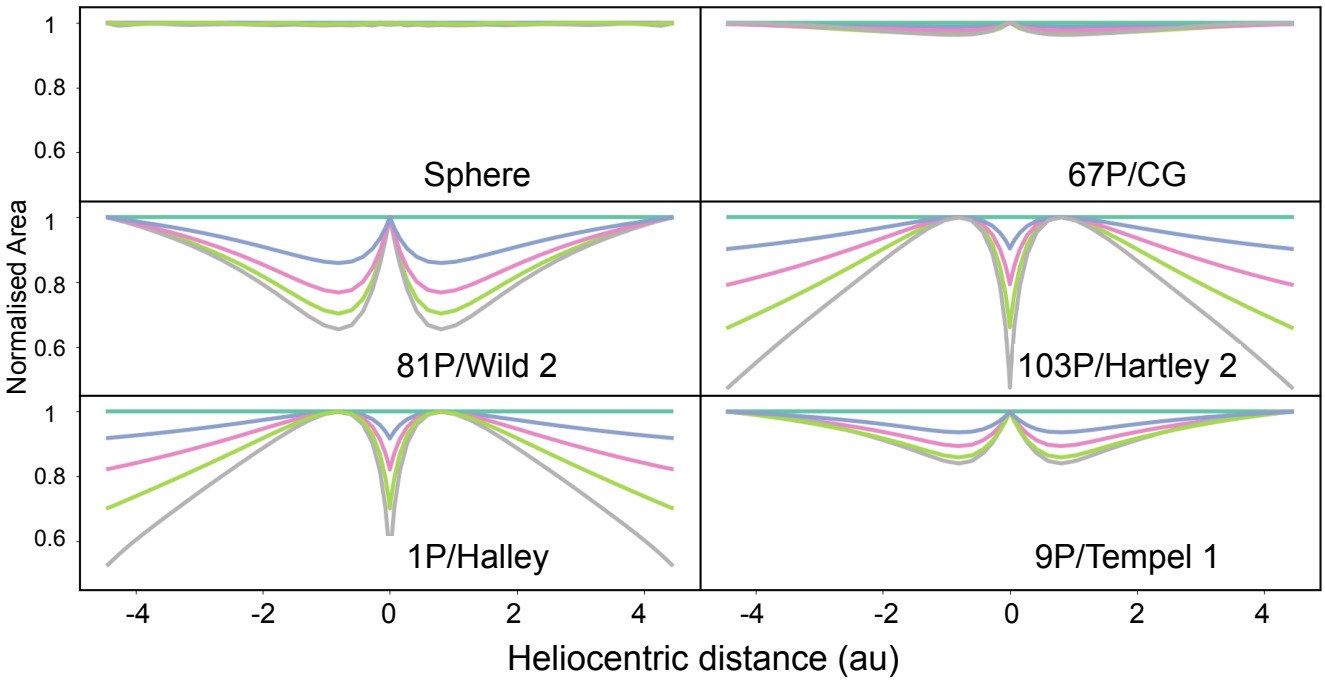

Fig. 1. Change in the normalised cross section of the illuminated area for six selected comet shapes (sphere, 67P, 81P, 103P, 1P, and 9P) at five different obliquities (0°, 30°, 45°, 60° , and 90°) with distance in au from perihelion (on a 67P-like orbit, perihelion occurs at 1.24 au).

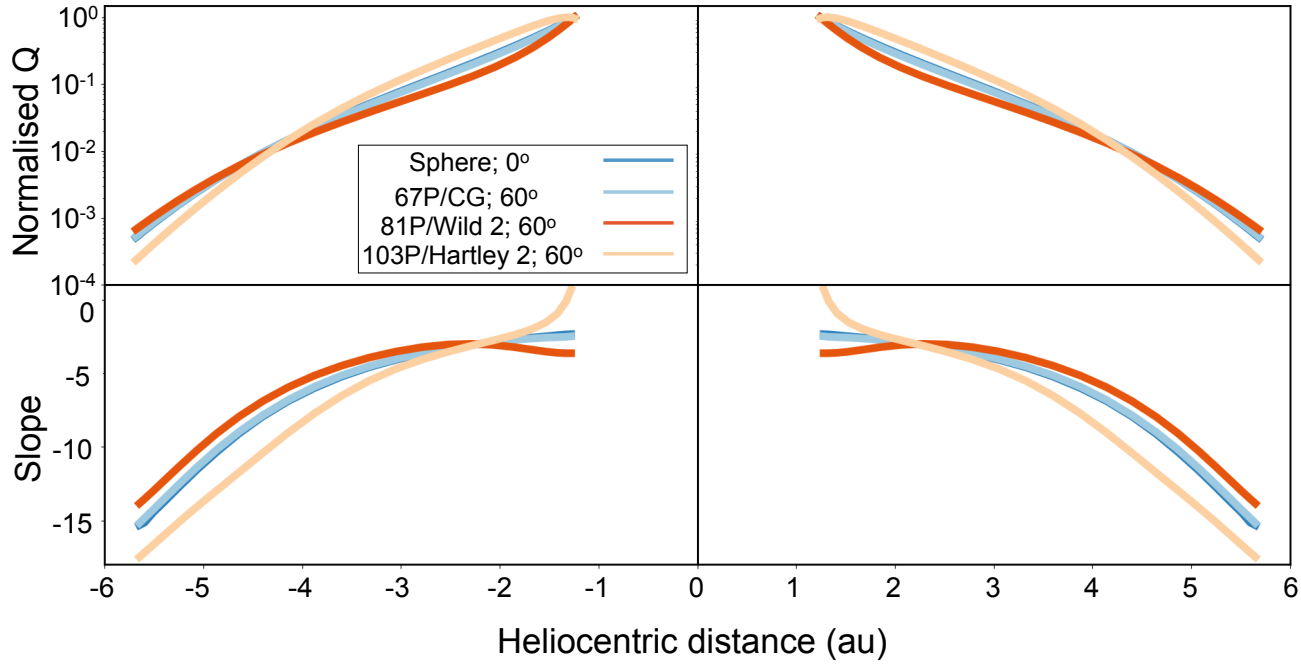

Fig. 2. Normalised water production rate and slopes of differently shaped comets (sphere, 67P, 81P, 103P). A sphere with an obliquity of 0° is shown as a reference. Any shape at 0° has a similar production rate curve. Comets 67P, 81P, and 103P are shown at obliquities of 60°. *Left and right panels*: pre- and post-perihelion, respectively. Pre-perihelion distances are denoted as negative and post-perihelion distances are given as positive. For a 67P-like orbit, perihelion occurs at 1.24 au (or −1.24 au in the pre-perihelion figures on the left).

3.2. Effect of activity distributions

In the previous section, we considered all the surface of the comet to be active. This is unlikely to apply in reality. For example, Keller et al. (2015) and Marschall et al. (2016) show that only certain local activity can explain the outgassing observations of 67P. In this section, we show how features in the production rate curves and their slopes are affected by random and non-random distributions of active regions on the comet. We examined the production rate curves for six different distributions of activity on a sphere: 100% active, 50% randomly distributed activity, 20% randomly distributed activity, an active region on the northern hemisphere, an active region on the southern hemisphere, and an active belt at 0° longitude.

For an obliquity of 0°, all the distributions produced similar production rate curves; only the absolute value of Q is affected.

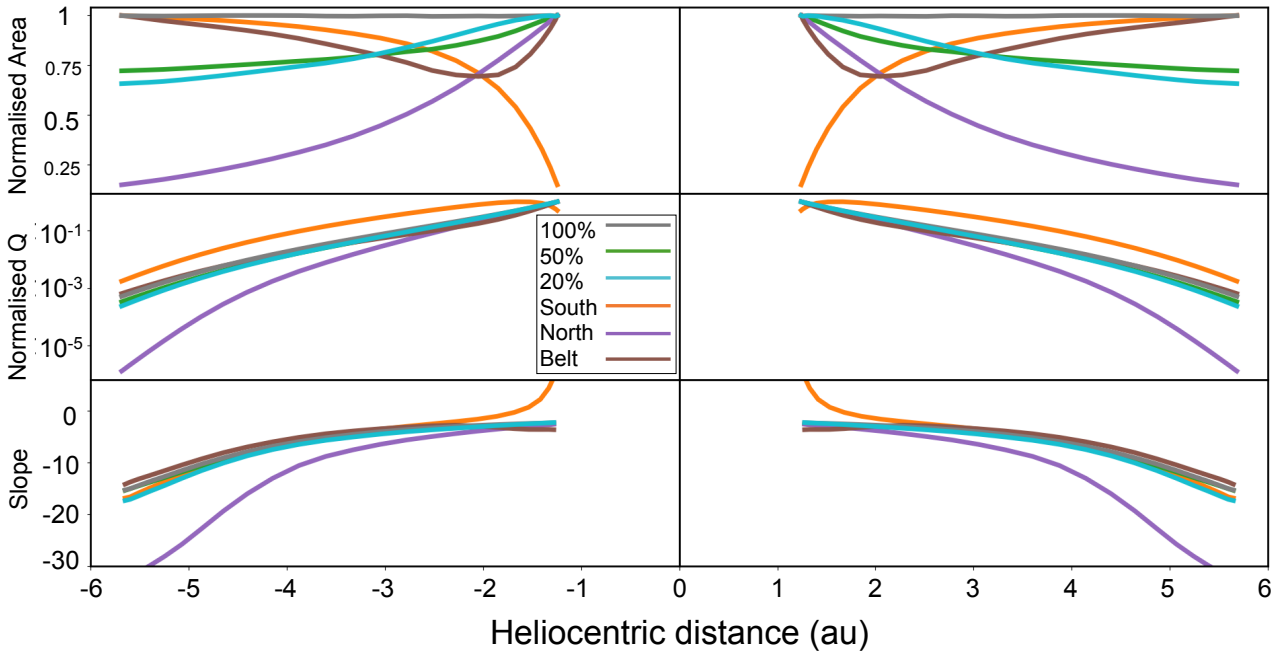

Fig. 3. Normalised area, water production rate, and slopes of spherically shaped comets with different distributions of activity (100% active, 50% active, 20% active, active region on the north hemisphere, active region on the southern hemisphere, active belt at 0° longitude) at 60° obliquity.

The illuminated area stays constant with heliocentric distance and only the magnitude changes depending on how much of the surface is active.

For an obliquity of 60° though, there are significant differences between the production rate curves for each kind of distribution. These are shown in Fig. 3. In the two randomly distributed cases, the illuminated areas are reasonably constant although they can have fluctuations based on how the random activity is distributed. As expected, these fluctuations do not change the production rate curves much and slopes are comparable to the fully active case.

When considering an active region on the northern side, the illuminated area increases dramatically as the comet approaches perihelion, but remains on the night side for long period going to aphelion due to the assumed obliquity of the rotation axis. The production rate slope starts out very steep, but around perihelion the curve and slope are comparable to the randomly distributed cases. When the active region is on the southern side, the opposite happens. The active region faces the Sun at aphelion and is away from the Sun at perihelion. Hence, the illuminated area decreases with heliocentric distance and the slope is therefore less steep at perihelion and becomes positive. The peak in production is offset before and after perihelion.

In the final case, activity is confined to a belt at 0° longitude. Here, the illuminated area decreases until it reaches a minimum and then increases towards perihelion. This is identical in behaviour to a fully active comet shaped like Wild 2, and both of their production rate curves behave in the same way, with a significant steepening at perihelion. This shows that a sphere with a defined region of activity can have the same production rate curve as an irregularly shaped fully active comet. As a result, it is difficult to disentangle the effects of shape and activity from only the production rate curves.

3.3. Effects of obliquity and Φ

In all the simulations so far, the pre- and post-perihelion curves have been symmetrical around perihelion. This is because the obliquity angle has always been orientated towards perihelion (parallel to the semi-major axis), so the change in illuminated area during approach and recession is symmetrical. We now introduce the argument Φ, as defined in Sect. 2. Its effects are actually well known in dealing with light curves of asteroids and comet brightness observations. Here we show that variations in Φ also have a strong effect on the production rate curves.

We show four selected examples in Fig. 4 to illustrate the main point for a 103P/Hartley 2 shaped comet: an obliquity of 0° and an argument Φ of 60°; an obliquity of 60° and an argument Φ of 90°; an obliquity of 60° and an argument Φ of 60°; and an obliquity of 80° and an argument Φ of 10°. For the first case, there is no change in the illuminated area. The argument Φ changes the angle between the rotation axis and the semi-major axis, but as the obliquity angle is zero, the rotation axis is still perpendicular to the orbital plane. As a result, the illuminated cross section does not change with heliocentric distance and the production curves remain unaltered.

With an obliquity of 60° and argument Φ of 90°, the change in illuminated area is the inverse of the change for 103P/Hartley 2 in Sect. 3.1, which also had an obliquity of 60°. Argument Φ orients the rotation axis away from the comet-sun vector at perihelion/aphelion, rather than in the same direction, as in Sect. 3.1. Now the area decreases with heliocentric distance before increasing at perihelion. This has the effect of creating a steep production rate curve around perihelion, similar to the case of Wild 2 in Fig. 2. Importantly, differently shaped comets can be seen to have a similar behaviour in their production rate slopes for different values of Φ. The pre- and post-perihelion curves are still symmetric around perihelion though.

Asymmetry in the water production can be produced for other values of obliquity and argument Φ. With the obliquity at 60° and the argument Φ at 60°, a slight offset can be seen, moving the peak production from 1.24 au (perihelion) to 1.26 au post-perihelion, equivalent to a delay of approximately 16 days. The increase in area post-perihelion is large enough to compensate for the loss of flux from moving out to larger heliocentric distances.

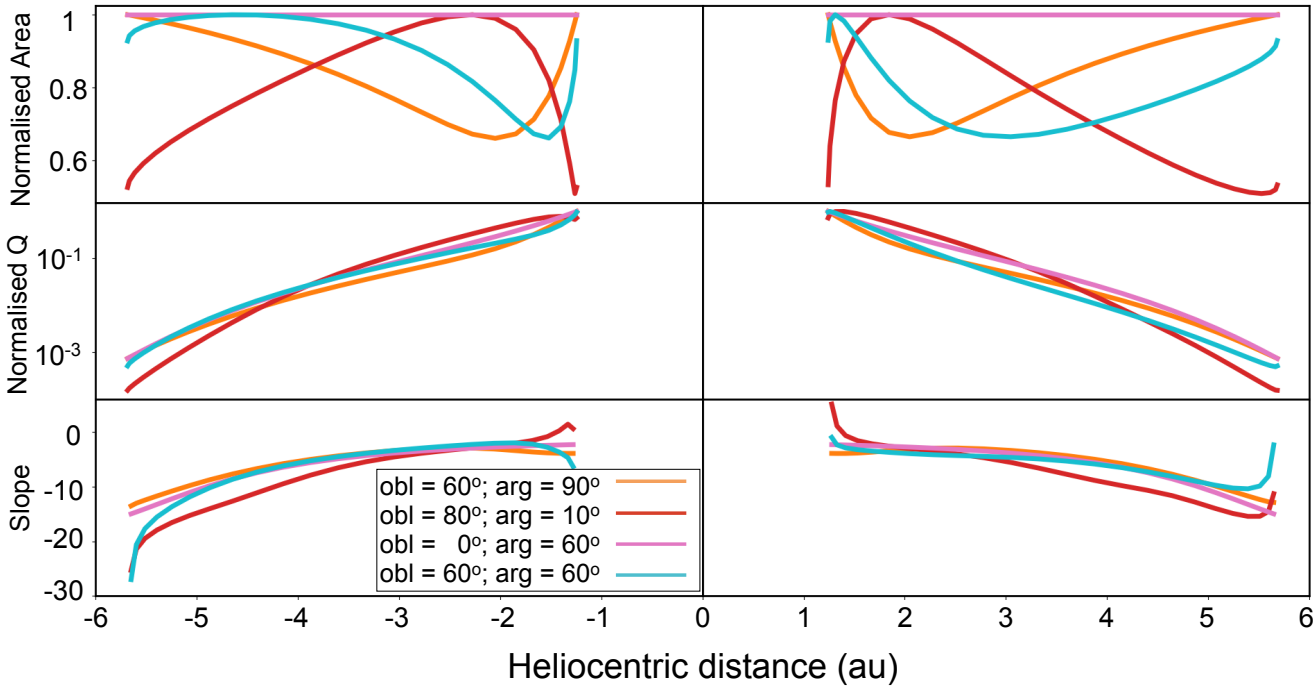

Fig. 4. Normalised area, water production rate and slopes of 103P/Hartley 2 shaped comets with different obliquities and Φ angles (obliquity = 0°, Φ = 60°; obliquity = 60°, Φ = 60°; obliquity = 80°, Φ = 10°). The pre- and post-perihelion curves are plotted on the *left and right panels*, respectively.

Finally, for the case of an obliquity of 80° and Φ of 10°, peaks in the production rate can be seen pre- and post-perihelion as the illuminated area reaches a maximum before and afterwards. The peak production can now be seen at 1.4 au pre- and post-perihelion, shifting by about 50 days from the closest approach.

Our modelling is incapable of producing an offset in water production for 67P for an obliquity of 52° and argument Φ of 20°, the estimated values for 67P. This is due to the nearly constants behaviour of the illuminated cross section with heliocentric distance. There is not a sufficient increase in area to overcome the decreasing amount of flux received as heliocentric distance increases. A defined active region would have to be used to create an offset in our model.

4. Conclusions

We applied a simplified model of water outgassing rate for different cometary bodies to investigate how cometary nucleus shape, spin axis orientation, and activity distribution determine the observable dependence with heliocentric distance. We acknowledge that our modelling relies on strong simplifications and does not correspond to any realistic cometary object. Using an assumption of ice on the surface, we are neglecting processes like thermal conductivity (through a dust layer), temperature-dependent sublimation coefficient, and a number of other physical processes. This means that our water production curves should not be viewed as explanatory of any observation, or as an accurate prediction. Our motivation is to use the idealised model as a tool to unambiguously isolate the effects of nucleus shape and spin axis orientation on relative heliocentric production rates.

The 67P/CG shape model has errors of ±0.3 m across the whole surface (Preusker et al. 2015). The shape model for 103P has errors of ±10 m in the areas constrained by stereo observations and errors of ±30 m in the less observed areas (Thomas et al. 2013). The 9P/Tempel shape has an average uncertainty <30 m across the whole surface (A'Hearn et al. 2005). For 81P/Wild, the uncertainty is around tens of metres in the well-observed regions and higher elsewhere (Li et al. 2009). The resolutions of these shape models are good enough to show the strong effect of shape on the water production rate curve, but there are a number of uncertainties relating to the unobserved parts of the nucleus. If the nucleus shape is significantly different to what has been assumed (possibly due to some unseen convexity or unusual topography), then the change in illuminated area would be different and thus the water production rate curves will be different from what we find. This problem only underlines our central argument; without knowing the exact shape, it is impossible to properly interpret the nature of comet outgassing from just the production rate curve alone.

Nevertheless, even in this idealistic form it is sufficient to demonstrate the importance of the investigated parameters on the heliocentric production rates of water within 3 au (i.e. spin-axis orientation, shape effects, and activity distribution). The application of more comprehensive and detailed models (accounting for self-heating, shadowing, gas diffusion through porous dust mantles with moving boundary, depth variation of conductivity, micro-fracturing, re-condensation effects, perhaps ice-crystallisation, and a number of other effects) is beyond the scope of this work, but they clearly merit future investigations for objects where at least the basic nucleus shape and spin-axis orientation are known. This point is exemplified by the current modelling effort trying to understand the 67P/CG heliocentric production rate, where none of the sophisticated models can yet account for all the characteristics of the water variation with time (for example Keller et al. 2015; Hu et al. 2017; Blum et al. 2017). In the introduction we asked: Is there a qualitative and/or quantitative way to interpret the behaviour of $Q(r_h)$ of a comet (for which the exact shape, spin axis, and activity distribution are not known), and how can we extract meaningful inter-comparisons of such observations for different comets?

The following general conclusions follow from the presented results:

- For homogeneous, solar driven activity, the illuminated cross section of the nucleus as it travels on its orbit governs the water production rate, $Q(r_h)$, and its gradient with heliocentric distance.
- This variability, even under an assumption of an homogeneous icy surface, is significantly modulated by the basic parameters: nucleus shape and spin axis orientation. For example, a comet shaped like 103P/Hartley 2 with a 90° obliquity produces changes in the illuminated cross section of 50% compared to 0° over an orbit, whereas changes of less than 20% are seen for a comet shaped like 9P/Tempel 1 at 90° obliquity.
- The often assumed (approximately) accurate $Q(r_h) \sim r^{-2}$ is valid only for homogeneously active objects at zero obliquity. This relationship holds only over a very narrow heliocentric range around 1 au.
- It is insufficient to derive a single value for the slope in the form $Q(r_h) = Ar_h^B$, over a large range of heliocentric distances (covering data beyond 3 au), as the slope, B, is also a function of distance. Even in the simplest case of a sphere with 0 degree obliquity, the production rate slope varies from a value of −4 at 3 au to −2.5 at 2 au. Therefore, intercomparisons of such values among different comets may not be informative.
- If there is a non-uniform distribution of active regions on a comet body (possibly due to any combination of dust cover/mantle, extended sources, albedo, and so on), virtually any shape of $Q(r_h)$ can be obtained. This is especially true for irregularly shaped objects with non-zero axis obliquity and Φ angle.
- The axis orientation (obliquity and Φ) is a sufficient condition for irregular shapes to yield asymmetric $Q(r_h)$ and its slopes. The strength of this effect is modulated by the nucleus shape (illuminated cross section variations).

Inferring physical properties of (unresolved) comets from their production rate curves is an exceptionally difficult task and caution should be exercised when interpreting these curves.

The above conclusions have strong implications for intercomparisons of the $Q(r_h)$ for different comets, especially when nucleus shape and spin axis orientation are not known. We argue that direct comparison of slopes of heliocentric production rates obtained from different distances as well as mixing pre- and post-perihelion data make it very difficult to draw consistent conclusions. It is not rare that such comparisons are published in the literature (usually a result of observational constraints), with one recent example in Wedlund et al. (2016). Such comparisons, as shown in this work, cannot be physically meaningful except by chance.

Finally, a suitable example where the shape and spin axis orientation is well determined but the slope of $Q(r_h)[H_2O]$ does not obey the r_h^{-2} approximation is the comet 67P. This is surprising, since it retains nearly a constant cross section despite its spin axis orientation throughout its orbit, as shown. From Rosetta measurements, the production rate slope ranges from −3 to −8 (Hansen et al. 2016; Marshall et al. 2017), which based on our results can be explained only by an inhomogeneous distribution of water activity. Observations from MIRO and ROSINA (Rosetta Orbiter Spectrometer for Ion and Neutral Analysis) have already implied that the activity is not homogeneously distributed, with activity in particular regions being stronger than in other areas (Marshall et al. 2017; Marschall et al. 2016; Fougere et al. 2016). The observed delay in peak production rate for 67P (Hansen et al. 2016; Marshall et al. 2017; Bondarenko & Medvedev 2011) must be a combination of the factors described here, or additional processes not considered. Applying more sophisticated models to detailed observations of 67P may provide a better fit, but to what degree such a fit is unique is still open. This fact only underlines our general argument using a simple model.

Acknowledgements. D.M. has received funding from the European Union's Horizon 2020 research and innovation programme under grant agreement No 686709. This work was supported by the Swiss State Secretariat for Education, Research and Innovation (SERI) under contract number 16.0008-2. The opinions expressed and arguments employed herein do not necessarily reflect the official view of the Swiss Government. L.R. was supported from the DFG project RE 3813/1–1. Y.Z. thanks the National Natural Science Foundation of China (Grant No: 11761131008, 11673072). We are very thankful to H. U. Keller and Y. Skorov for encouragement to work on this topic, and all the helpful discussions. The shape models used here were downloaded from the 3D Asteroid Catalogue: https://space.frieger.com/asteroids/comets/ Deutsche Forschungsgemeinschaft, DFG project number Ts 17/2–1.

References

A'Hearn, M. F., Belton, M., Delamere, W., et al. 2005, Science, 310, 258
Biver, N., Bockelée-Morvan, D., Colom, P., et al. 1997, Earth Moon Planets, 78, 5
Blum, J., Gundlach, B., Krause, M., et al. 2017, MNRAS, 469, S755
Bockelée-Morvan, D., Gautier, D., Hersant, F., Huré, J.-M., & Robert, F. 2002, A&A, 384, 1107
Bockelée-Morvan, D., Biver, N., Crovisier, J., et al. 2010, BAAS, 42, 946
Bondarenko, Y. S., & Medvedev, Y. D. 2011, Solar Syst. Res., 45, 330
Cowan, J. J., & A'Hearn, M. F. 1979, Moon Planets, 21, 155
Fanale, F. P., & Salvail, J. R. 1984, Icarus, 60, 476
Farnham, T., & Thomas, P. 2013a, PLATE SHAPE MODEL OF COMET 103P/HARTLEY 2 V1. 0, Tech. rep., DIF-C-HRIV/MRI-5-HARTLEY2-SHAPE-V1.0, NASA Planetary Data System
Farnham, T., & Thomas, P. 2013b, PLATE SHAPE MODEL OF COMET 9P/TEMPEL 1 V2. 0, Tech. rep., DIF-C-HRIV/ITS/MRI-5-TEMPEL1-SHAPE-MODEL-V2.0, NASA Planetary Data System
Farnham, T., Duxbury, T., & Li, J. 2005, Shape Models of Comet Wild 2, Tech. rep., SDU-CNAVCAM-5-WILD2-SHAPE-MODEL-V2. 0, NASA Planetary Data System
Fougere, N., Altwegg, K., Berthelier, J.-J., et al. 2016, A&A, 588, A134
Gundlach, B., Skorov, Y. V., & Blum, J. 2011, Icarus, 213, 710
Hansen, K. C., Altwegg, K., Berthelier, J.-J., et al. 2016, MNRAS, 462, S491
Hässig, M., Altwegg, K., Balsiger, H., et al. 2015, Science, 347, aaa0276
Hu, X., Shi, X., Sierks, H., et al. 2017, MNRAS, 469, S295
Keller, H. U., Mottola, S., Davidsson, B., et al. 2015, A&A, 583, A34
Kossacki, K. J., Markiewicz, W. J., Skorov, Y., & Kömle., N.I. 1999, Planet. Space Sci., 47, 1521
Kührt, E. 1999, Space Sci. Rev., 90, 75
Laeuter, M., Kramer, T., Rubin, M., & Altwegg, K. 2019, MNRAS, 483, 852
Lamy, P. L., Toth, I., Davidsson, B. J., et al. 2007, Space Sci. Rev., 128, 23
Langmuir, I. 1913, Phys. Rev., 2, 329
Li, J.-Y., A'Hearn, M. F., Farnham, T. L., & McFadden, L. A. 2009, Icarus, 204, 209
Marschall, R., Su, C., Liao, Y., et al. 2016, A&A, 589, A90
Marshall, D., Hartogh, P., Rezac, L., et al. 2017, A&A, 603, A87
Meech, K., Svoren, J., Festou, M., Keller, H., & Weaver, H. 2004, Comets II (Tucson, AZ: University of Arizona Press)
Preusker, F., Scholten, F., Matz, K.-D., et al. 2015, A&A, 583, A33
Russo, N. D., Mumma, M. J., DiSanti, M. A., et al. 2000, Icarus, 143, 324
Russo, N. D., DiSanti, M. A., Magee-Sauer, K., et al. 2004, Icarus, 168, 186
Sekanina, Z. 1981, Ann. Rev. Earth Planet. Sci., 9, 113
Skorov, Y. V., Rezac, L., Hartogh, P., & Keller, H. U. 2017, A&A, 600, A142
Steckloff, J. K., & Jacobson, S. A. 2016, Icarus, 264, 160
Steckloff, J. K., Johnson, B. C., Bowling, T., et al. 2015, Icarus, 258, 430
Stooke, P. 2002, NASA Planetary Data System, 166
Thomas, P., A'Hearn, M. F., Veverka, J., et al. 2013, Icarus, 222, 550
Watson, K., Murray, B. C., & Brown, H. 1962, Icarus, 1, 317
Wedlund, C. S., Kallio, E., Alho, M., et al. 2016, A&A, 587, A154
Weissman, P. R., & Kieffer, H. H. 1981, Icarus, 47, 302
Whipple, F. L. 1950, ApJ, 111, 375